Journal of Alloys and Compounds 522 (2012) 63–68

Contents lists available at SciVerse ScienceDirect

Journal of Alloys and Compounds

journal homepage: www.elsevier.com/locate/jallcom

Effect of Zn nanoparticles morphology on the photoelectrochemical properties of Zn/TiO_2NTs nanocomposites

Huichao He [a], Peng Xiao [b], Yunhuai Zhang [a,*], Yichao Jia [a], Yannan Yang [c], Zhengyang Qiao [a]

[a] College of Chemistry and Chemical Engineering, Chongqing University, Chongqing 400030, PR China
[b] College of Physics, Chongqing University, Chongqing 400030, PR China
[c] Environmental Monitoring Station of Ziyang, Ziyang 641300, PR China

ARTICLE INFO

Article history:
Received 11 November 2011
Received in revised form 4 January 2012
Accepted 15 January 2012
Available online 28 January 2012

Keywords:
Zinc nanoparticles
Titania nanotube
Photoelectrochemical property
Morphology

ABSTRACT

Zn nanoparticles with different size and distribution were loaded on/into TiO_2 nanotube arrays (Zn/TiO_2NTs) via pulsed electrodeposition method. The morphology of Zn/TiO_2NTs was studied by field emission scanning electron microscopy (FESEM). The morphology influence of Zn nanoparticles on the photoelectrochemical properties of Zn/TiO_2NTs were investigated by UV–vis diffuse reflectance spectrum (UV–vis DRS) and photoelectrochemical measurements. The results showed that Zn/TiO_2NTs composites with an average size at 40–50 nm and uniformly distributed of Zn nanoparticles possessed the narrowest band gap, the best photocurrent response, the highest charge carriers density and minimum charge-transfer resistance. These discrepancies in photoelectrochemical properties of different Zn/TiO_2NTs samples can be ascribed to the size and distribution effect (morphology effect) of Zn nanoparticles which can influence the transfer and separation of photo-induced carriers generated by TiO_2NTs.

© 2012 Elsevier B.V. All rights reserved.

1. Introduction

Highly ordered TiO_2 nanotube arrays (TiO_2NTs) prepared via anodic oxidation of titanium possess high surface-to-volume ratios and fast charge transport property, which are often considered to be advantageous for applications requiring efficient surface reactivity and photoelectric sensitivity, for example, photocatalytic and photoelectrochemical degradation of organic pollutants or sensor [1–3]. However, previous studies on the applications of TiO_2NTs have found that the high recombination rate of photogenerated electron–hole pairs and wide band gap ($E_g \approx 3.2$ eV) were the main drawbacks that limited the photocatalytic activity and visible light response of TiO_2NTs [4,5].

To overcome the drawbacks, several strategies have recently been reported, such as doping TiO_2NTs with metal cations and non-metal anions, combining TiO_2NTs with metal nanoparticles [6–8]. On the basis of metal–semiconductor contact theory, Schottky barrier can be formed at the contact interface between metal nanoparticles and TiO_2 when higher work function metals in contact with the TiO_2. Because of the existence of the inner electric field, the photo-induced electrons of TiO_2 can be transferred to the metal nanoparticles and then the opportunity of recombination of electron-hole pairs will be decreased [9,10]. Accordingly, TiO_2NTs loaded with higher work function metal nanoparticles is a feasible and effective way to improve the photoelectrochemical activity of TiO_2NTs.

At present, various metal nanoparticles loaded on TiO_2NTs have been reported [5,11,12]. However, most research focused on the preparation methods and general applications of metal/TiO_2NTs nanocomposites, the correlation between the photoelectrochemical properties of TiO_2NTs and the morphology of metal nanoparticles such as grain size, distribution properties were not well understood. Kamat and co-workers demonstrated that the size of gold nanoparticles have an influence on the charge distribution and Fermi level equilibration for TiO_2 powder [13]. On the other hand, studies for the photocatalytic degradation of pollutant found that the size and aggregation of metal nanoparticles have a distinct impact on the photocatalytic efficiency for TiO_2 powder [14,15]. These researches indicated that the photoelectrochemical activities of TiO_2NTs are associated with the size and distribution of metal nanoparticles on/into TiO_2NTs. Thus it is very important to investigate the influence of metal nanoparticles morphology on the photoelectrochemical properties of TiO_2NTs. However, until now, few researches were reported in this area.

In this work, Zn nanoparticles with different size and distribution were loaded on/into TiO_2NTs by pulsed electrodeposition method, and the influences of the morphology of Zn nanoparticles on the photoelectrochemical properties of TiO_2NTs were systematically investigated and discussed. This work may provide reference

* Corresponding author. Tel.: +86 13883077781; fax: +86 023 6510203.
E-mail addresses: hehuichao985@gmail.com (H. He), xp2031@163.com (Y. Zhang).

0925-8388/$ – see front matter © 2012 Elsevier B.V. All rights reserved.
doi:10.1016/j.jallcom.2012.01.077

and insights for designing and preparing highly photoelectrochemical activity metal/TiO_2NTs nanocomposites.

2. Experimental

2.1. Preparation of Zn/TiO_2NTs

TiO_2NTs were fabricated by electrochemical anodic oxidation in HF electrolyte. The growth conditions used in this work are similar to those reported in our early publications and this section was omitted here [16]. The as-grown TiO_2NTs subsequently were annealed in dry nitrogen environment at 450 °C for 2 h with heating and cooling rates of 5 °C min^{-1} to convert the amorphous TiO_2NTs to anatase phase. Pulsed electrodeposition method was employed to prepare the Zn nanoparticles on/into TiO_2NTs. The electrodeposition was carried out in a conventional three-electrode cell, the as-annealed TiO_2NTs served as the working electrode, and a saturated calomel electrode (SCE) and a platinum electrode served as the reference and counter electrode, respectively. The electrolyte was prepared by dissolving/analytical grades of $ZnCl_2$ (0.25 M) and H_3BO_3 (25 g L^{-1}) in deionized water. The pulsed electrodeposition was carried out at ±80 mA cm^{-2} of current density with 8–14 ms different cathodal current on-time (t_{on}), 1 ms anodic current on-time and 100 ms current off-time. The deposited charge density of all samples was fixed at 179.2 mC cm^{-2}. The pulsed potential signals are shown in Fig. 1.

2.2. Characterization and photoelectrochemical measurements

Field emission scanning electron microscopy (FESEM, Nova 400 Nano-SEM) was employed to characterize the morphology of TiO_2NTs and Zn/TiO_2NTs. The crystalline structure of the samples was identified by X-ray diffraction (XRD, Shimadzu ZD-3AX, Cu Kα radiation). And UV–visible diffuse reflection spectra measurements (UV-vis DRS, Hitachi U-3010 spectrophotometer) were performed with $BaSO_4$ as a reflectance standard. Photoelectrochemical measurements were carried out at room temperature with an electrochemical workstation (CHI660C, Shanghai, China). The pure TiO_2NTs and Zn/TiO_2NTs electrodes with an geometric area of 1.0 cm^2 was placed in the measurement as the working electrode, and an Ag/AgCl and platinum electrode served as the reference and counter electrode, respectively. A 500 W PLS-SXE300/300UV Xe lamp (320–780 nm) was used as light source and 0.01 M Na_2SO_4 aqueous solution as supporting electrolyte.

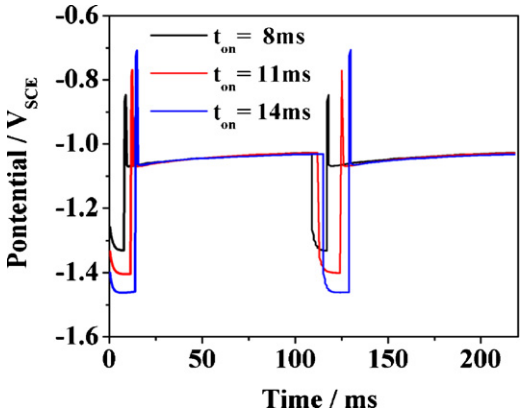

Fig. 1. The pulsed potential signals of Zn nanoparticles deposited at different t_{on}.

3. Results and discussion

3.1. Morphology and structure analysis

The top-view and cross-section of TiO_2NTs are shown in Fig. 2a, which reveals that the diameters of TiO_2NTs range from 80 to 100 nm and the average tube length is approximately 400 nm (inset of Fig. 2a). Fig. 2b–d presents the FESEM images of Zn nanoparticles loaded on/into TiO_2NTs at different t_{on} (8, 11, 14 ms), respectively. It can be observed that Zn nanoparticles with different size and distribution were loaded on/into TiO_2NTs. In addition, the average size of nanoparticles decreased gradually from 100 to 15 nm with the increasing t_{on} from 8 to 14 ms under the same deposited charge density. The maximum size distribution of Zn nanoparticles was averagely at 80–100 nm when t_{on} was 8 ms. The minimum

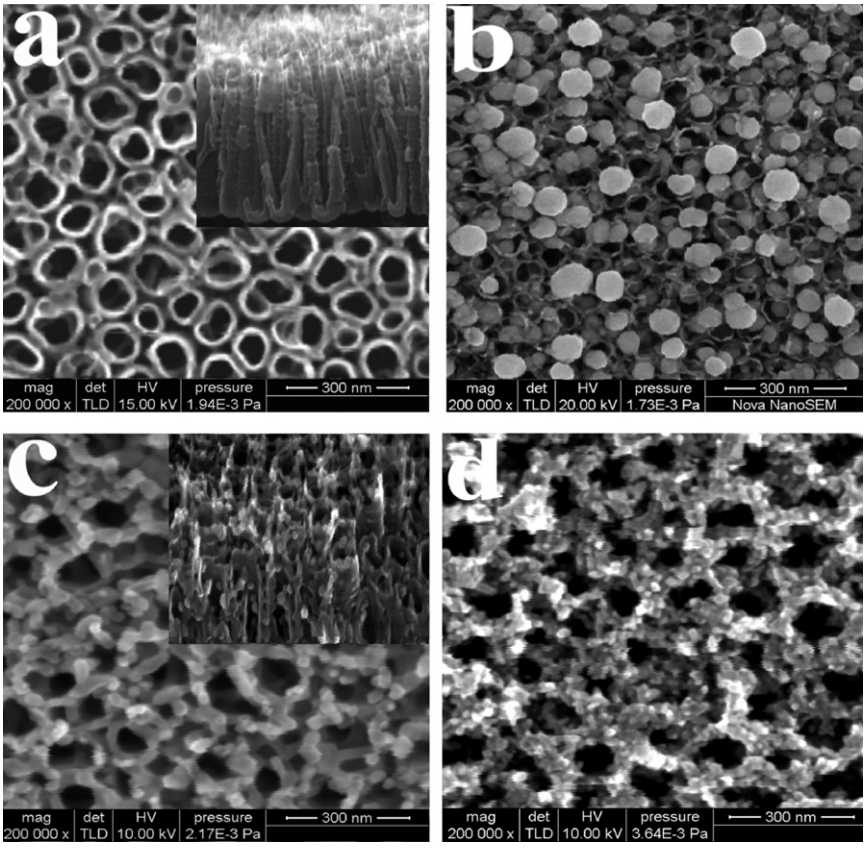

Fig. 2. FESEM images of (a) TiO_2NTs and Zn/TiO_2NTs prepared at (b) t_{on} = 8 ms, (c) t_{on} = 11 ms and (d) t_{on} = 14 ms.

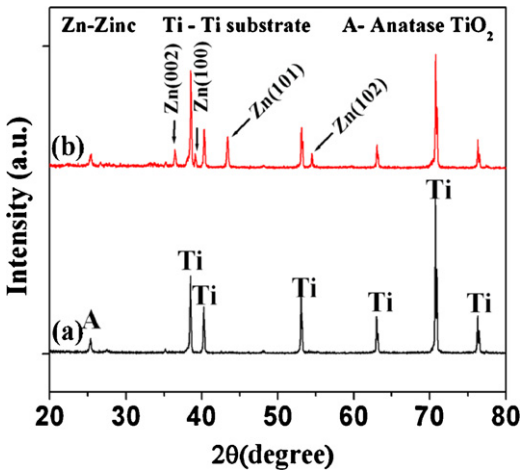

Fig. 3. XRD patterns of TiO_2NTs (a) and Zn/TiO_2NTs (b).

size distribution was averagely at 10–20 nm when t_{on} was 14 ms, moreover, these small particles were agglomerated together on the top of the TiO_2NTs. When t_{on} = 11 ms, the size of Zn nanoparticles were about 40–50 nm and uniformly distributed on/into the tubes (inset of Fig. 2c). The influence of t_{on} on the size of Zn nanoparticles can be contributed to the increasing number of Zn nucleation sites caused by higher negative overpotential at longer t_{on} [17]. The pulsed potential signals of the studied t_{on} are recorded in Fig. 1, which proved that higher negative overpotential can be obtained at a longer t_{on}.

The XRD patterns of TiO_2NTs (a) and Zn/TiO_2NTs (b) are shown in Fig. 3. Curve (a) demonstrates a regular anatase TiO_2NTs crystal structure, which is ascribed to the appearance of characteristic diffraction peaks at 2θ = 25.3°. In curves (b), Zn/TiO_2NTs exhibits not only the characteristic peak of anatase, but also four new characteristic peaks at 36.2°, 39.1°, 43.2° and 54.3°, corresponding to (0 0 2), (1 0 0), (1 0 1) and (1 0 2) facets of Zn, which indicates that Zn nanoparticles were deposited on TiO_2NTs successfully.

3.2. UV–vis DRS analysis

Fig. 4a shows the UV-vis DRS of pure TiO_2NTs and Zn/TiO_2NTs at room temperature. As demonstrated in Fig. 4a, compared with TiO_2NTs, Zn/TiO_2NTs samples present stronger absorption band in the range of 200–900 nm and the main absorption edge shift a little to the longer wavelength, indicating the narrowing of the band gap. In addition, for Zn/TiO_2NTs, a new absorption peak appears at 431 nm and the characteristic peak at 560 nm and 800 nm become broader, which may be attributed to the transverse plasma resonance effect of Zn nanoparticles [18]. The band gaps (E_g) can be estimated according to Eq. (1).

Table 1
The calculated band gaps of TiO_2NTs and Zn/TiO_2NTs.

Samples	Band gap (eV)
TiO_2NTs	3.23
Zn/TiO_2NTs (8 ms)	3.19
Zn/TiO_2NTs (11 ms)	3.14
Zn/TiO_2NTs (14 ms)	3.16

$$(\alpha h\nu)^n = A(h\nu - E_g) \quad (1)$$

where $h\nu$ is the incident photon energy, α is the absorption coefficient, and A is a constant. The value of n depends on the type of interband transition: n = 2 for an indirect transition and n = 1/2 for a direct transition. Plot of $(\alpha h\nu)^{1/2}$ versus $h\nu$ from the spectra data of TiO_2NTs and Zn/TiO_2NTs (t_{on} = 11 ms) in Fig. 4a are presented in Fig. 4b and c, the E_g estimated from the intercept of the tangents to the plot are 3.23 eV and 3.14 eV for TiO_2NTs and Zn/TiO_2NTs, respectively. With the same calculated method, E_g of the others Zn/TiO_2NTs were estimated. The calculated results are listed in Table 1.

The slight red shift of E_g on Zn/TiO_2NTs may be owing to the impact of Zn nanoparticles on the surface state of TiO_2NTs and ZnO formed on the Zn particle surface, which result in heterojunction structure formed at the interface between ZnO and TiO_2NTs [19,20]. For the Zn/TiO_2NTs, the discrepancy in E_g and absorption edges suggest that the optical property was influenced by the grain size and distribution properties of Zn nanoparticles, which in turn caused different contact interface between Zn nanoparticles and TiO_2NTs, leading to the shifting of Fermi level for Zn/TiO_2NTs [13]. As shown in Fig. 2c, Zn nanoparticles with a suitable size distribution on TiO_2NTs presented the strongest absorption band and narrowest E_g.

3.3. Photoelectrochemical properties

3.3.1. Photocurrent response

The separated efficiency of photogenerated electron–hole pairs in TiO_2NTs and Zn/TiO_2NTs was assessed by photocurrent response experiment. As shown in Fig. 5, the current responses on both TiO_2NTs and Zn/TiO_2NTs in the dark was relatively insignificant, while under illumination the electrons and holes were generated, and therefore the photocurrent densities were evidently increased. In comparison with TiO_2NTs, Zn/TiO_2NTs samples displayed much more intensive photocurrent responses, which indicated that the photogenerated electrons and holes in the Zn/TiO_2NTs can be separated more effective than that in TiO_2NTs. The enhancement

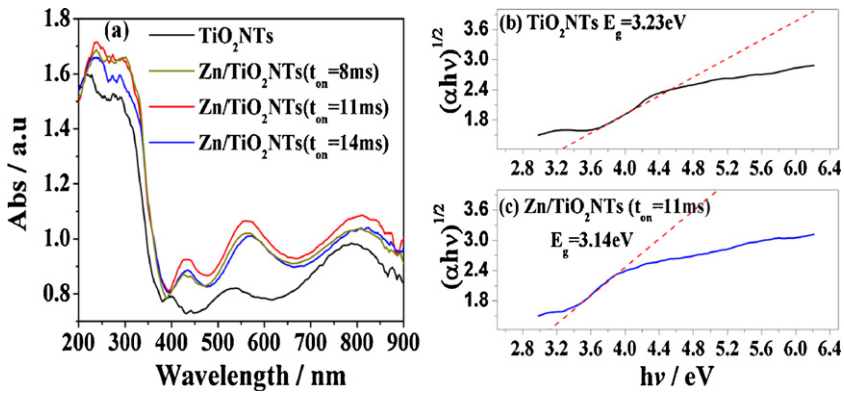

Fig. 4. (a) UV–vis DRS of TiO_2NTs and Zn/TiO_2NTs, polt of $(\alpha h\nu)^{1/2}$ vs. photon energy of (b) TiO_2NTs and (c) Zn/TiO_2NTs (t_{on} = 11 ms).

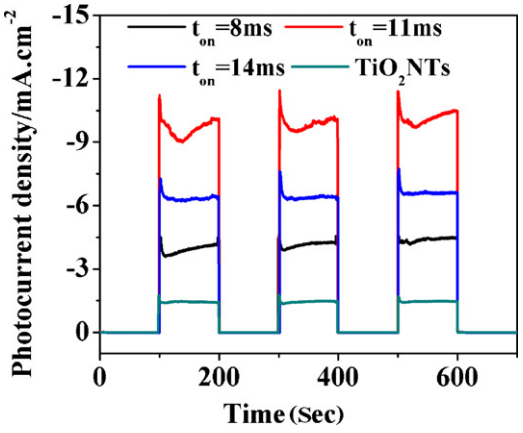

Fig. 5. Photocurrent responses of TiO_2NTs and Zn/TiO_2NTs at 0.6 V under pulsed-irradiation.

of separated efficiency was contributed to the Schottky barriers formed at the interface between Zn nanoparticles and TiO_2NTs. The Zn nanoparticles acted as sinks for photogenerated charge carriers, and promote interfacial charge-transfer processes in the composite systems [9,10]. In addition, different photocurrent densities were observed for Zn/TiO_2NTs prepared at different t_{on}. The sample which have appropriately dispersed Zn nanoparticles (t_{on} = 11 ms) exhibited the highest photocurrent density (about 10 mA cm^{-2}), which suggested that appropriately dispersed distribution of Zn nanoparticles was beneficial to the separation of photogenerated electron–hole pairs.

3.3.2. Mott–Schottky analysis

In order to evaluate the intrinsic electronic properties of the samples, Mott–Schottky analysis was performed by measuring the changes in the capacitance (C) as a function of the potential (V) in 0.01 M Na_2SO_4 solution. The data of C–V can be used for evaluating the flat band potential and the charge carriers density by means of Mott–Schottky Eq. (2) [21,22].

$$C^{-2} = \frac{2}{\varepsilon\varepsilon_0 eN}\left(V - V_{fb} - \frac{kT}{e}\right) \quad (2)$$

where C is the total capacitance of the space charge region, ε is the dielectric constant of the material, ε_0 is the permittivity of the vacuum, e is the element charge, N is the concentration of charge carriers, V is the potential, V_{fb} is the flat band potential, k is the Boltzmann's constant, and T is the temperature (room temperature, ~298 K).

Table 2
The charge carriers density and flat band potential of TiO_2NTs and Zn/TiO_2NTs.

Samples	Charge carriers density (cm^{-3})	Flat band potential (V)
TiO_2NTs	1.72e+19	−0.032
Zn/TiO_2NTs (8 ms)	1.51e+20	−0.250
Zn/TiO_2NTs (11 ms)	2.49e+20	−0.427
Zn/TiO_2NTs (14 ms)	1.70e+20	−0.386

Fig. 6 presents the Mott–Schottky curves ($1/C^2$ vs. V) of different samples under irradiation. The $1/C^2$–V curves were in accordance with the expected behavior of n-type semiconductor under increased applied bias, i.e. a sharp decrease in the capacitance when the applied bias was increased inducing the generation of electron–hole pairs [22]. In each curve, a linear region and the direct proportionality between the inverse squared capacitance and the applied bias can be identified. Compared with Zn/TiO_2NTs, TiO_2NTs exhibited a non-linear bending character in the potential range, suggesting the pure TiO_2NTs were more insulating. On the other hand, each slope of different Zn/TiO_2NTs were different, which implied that the discrepancy in conductivity. The charge carriers density and flat band potentials were calculated and summarized in Table 2. It was shown that the Zn/TiO_2NTs exhibited a negative shift in the flat band potential in comparison with TiO_2NTs, which can be attributed to the equilibration of Fermi level between Zn and TiO_2 [9,10,13]. Higher charge carriers density on Zn/TiO_2NTs was due to the effectively trapping of photogenerated electrons for Zn nanoparticles. On the other hand, for different Zn/TiO_2NTs, Zn/TiO_2NTs prepared at t_{on} = 11 ms exhibited the highest charge carriers density and the most negative flat band potential. This result hinted again the separated efficiency of photogenerated electron–hole pairs was affected by the size and distribution of Zn nanoparticles.

3.3.3. Impedance analysis

The electrons transferring property of TiO_2NTs and Zn/TiO_2NTs was evaluated by electrochemical impedance spectroscopy (EIS). Fig. 7 shows the impedance spectra in the form of Nyquist plots for the samples measured at 0 V in the dark. All impedance spectra typically displayed a pronounced semicircle in the measured frequency region, which was attributed to the electron transfer process at the electrode/electrolyte interface and the radius corresponded to the electron-transfer resistance controlling the kinetics at the electrode interface [23]. The semicircle radius on the EIS Nynquist plots of Zn/TiO_2NTs were smaller than that of TiO_2NTs, suggesting a faster interfacial charge transfer occurred on the Zn/TiO_2NTs due to the presence of Zn nanoparticles. In addition, significant differences in the semicircle radius were observed for different Zn/TiO_2NTs. This

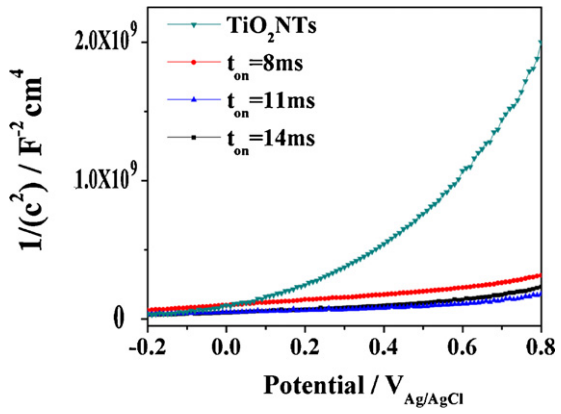

Fig. 6. Mott–Schottky plots of TiO_2NTs and Zn/TiO_2NTs under illumination.

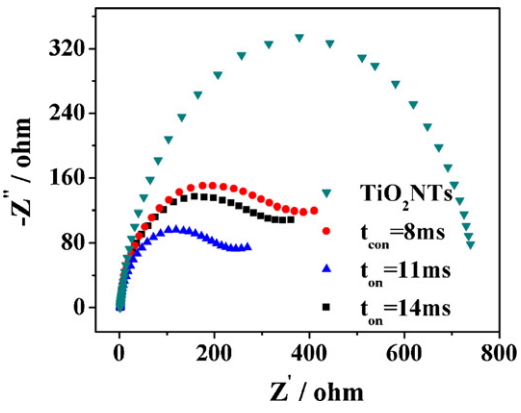

Fig. 7. EIS Nynquist plots of TiO_2NTs and Zn/TiO_2NTs in the dark.

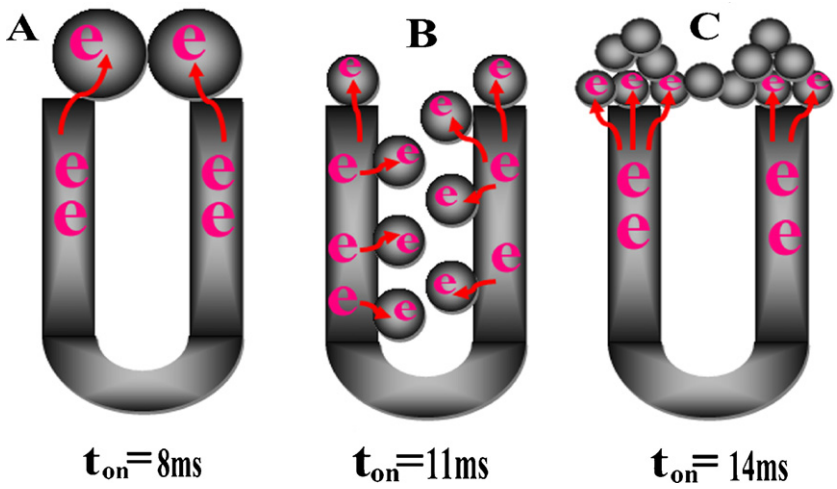

Fig. 8. Schematic diagram of the Zn nanoparticles loaded on TiO_2NTs and the electrons transfer and separation between the contact interfaces of Zn nanoparticles and TiO_2NTs.

implied the resistance of Zn/TiO_2NTs was affected by the distribution and particles size of Zn nanoparticles. The Zn/TiO_2NTs prepared at t_{on} = 11 ms owned the smallest semicircle radius of Nyquist plots which meant the fastest electrons transferring properties.

All the photoelectrochemical results indicated that the size and distribution of loaded Zn nanoparticles were the main reason that caused the discrepancies in photoelectrochemical properties on Zn/TiO_2NTs. These discrepancies are related to the separation and transfer of carriers between Zn nanoparticles and TiO_2NTs, the process were shown in Fig. 8. As electron sinks, Zn nanoparticles can isolate and transfer electrons from the TiO_2NTs through the Schottky contacts. Thus the transferred and separated efficiency were influenced by the contact interface between Zn nanoparticles and TiO_2NTs (shown in Fig. 8). The appropriately dispersed Zn nanoparticles can generate abundant contact interfaces between these nanoparticles and TiO_2NTs which in turn was helpful for the separation and transmission of carriers (Fig. 8; t_{on} = 11 ms). On the other hand, less contact interfaces between Zn nanoparticles and TiO_2NTs were formed when big (Fig. 8; t_{on} = 8 ms) or agglomerated (Fig. 8; t_{on} = 14 ms) Zn nanoparticles loaded on TiO_2NTs, which intrinsically lead to high recombination probability of electrons and holes and discontinuous electrons transfer [24]. In addition, it has been reported that the work function of metal was influenced by the particle size. If the size of metal particles was too large, its energetic properties may approach to that of bulk. The work function of metals would be decreased, and then electron could not be transferred effectively [25]. Compared with the sample B (t_{on} = 11 ms), the Zn particles of sample A (t_{on} = 8 ms) had bigger size and distribution and were only deposited on the top of TiO_2NTs, thus the carriers separation and transmission were decreased. The smaller Zn nanoparticles of sample C (t_{on} = 14 ms) were easy to agglomerate, which resulted in less contact interfaces between Zn nanoparticles and TiO_2NTs and the increase of transmission resistance of the carriers. Moreover, the work function of agglomerated Zn nanoparticles was similar to that of bulk, which also had impact on the transferred efficiency of carriers. Hence, the optimal photoelectrochemical properties of Zn/TiO_2NTs was presented when Zn nanoparticles were appropriately dispersed on/into TiO_2NTs (t_{on} = 11 ms).

4. Conclusions

In this paper, Zn nanoparticles with different size and distribution were loaded on/into TiO_2 nanotube arrays by pulsed electrodeposition method. The influences of morphology of Zn nanoparticles on the photoelectrochemical properties of Zn/TiO_2NTs were investigated. The results showed that the size and distribution effect of Zn nanoparticles played a crucial role in the transfer and separation of carriers. The optimal photoelectrochemical properties was registered in the case of Zn/TiO_2NTs prepared at t_{on} = 11 ms due to the moderate size (40–50 nm) and distribution Zn nanoparticles loaded on/into TiO_2NTs forming abundant contact interfaces between Zn nanoparticles and TiO_2NTs which can transfer and separate carriers effectively. The present work provide reference and insights for designing and preparing highly photoelectrochemical activity metal/TiO_2NTs nanocomposites.

Acknowledgment

This work was supported by the Fundamental Research Funds for the Central Universities (Project No. CDJXS11221174).

References

[1] Y.K. Lai, L. Sun, Y.C. Chen, H.F. Zhuang, C.J. Lin, J.W. Chin, J. Electrochem. Soc. 153 (2006) D123–D127.
[2] Z. Liu, X. Zhang, S. Nishimoto, M. Jin, D.A. Tryk, T. Murakami, A. Fujishima, J. Phys. Chem. C 112 (2008) 253–259.
[3] Q. Zheng, B.X. Zhou, J. Bai, L.H. Li, Z.J. Jin, J.L. Zhang, J.H. Li, Y.B. Liu, W.M. Cai, X.Y. Zhu, Adv. Mater. 20 (2008) 1044–1049.
[4] N. Lu, X. Quan, J.Y. Li, S. Chen, H.T. Yu, G.H. Chen, J. Phys. Chem. C 111 (2007) 11836–11842.
[5] I. Paramasivam, J.M. Macak, P. Schmuki, Electrochem. Commun. 10 (2008) 71–75.
[6] L. Sun, J. Li, C.L. Wang, S.F. Li, H.B. Chen, C.J. Lin, Sol. Energy Mater. Sol. C 93 (2009) 1875–1880.
[7] G.K. Mor, K. Shankar, M. Paulose, O.K. Varghese, C.A. Grimes, Nano. Lett. 5 (2005) 191–195.
[8] I. Paramasivam, J.M. Macak, A. Ghicov, P. Schmuki, Chem. Phys. Lett. 445 (2007) 233–237.
[9] T. Ioannides, X.E. Verykios, J. Catal. 161 (1996) 560–569.
[10] V. Subramanian, E. Wolf, P.V. Kamat, J. Phys. Chem. B 105 (2001) 11439–11446.
[11] K.P. Xie, L. Sun, C.L. Wang, Y.K. Lai, M.K. Wang, H.B. Chen, C.J. Lin, Electrochim. Acta 55 (2010) 7211–7218.
[12] A. Honciuc, M. Laurin, S. Albu, M. Amende, M. Sobota, R. Lynch, P. Schmuki, J. Libuda, J. Phys. Chem. C 114 (2010) 20146–20154.
[13] V. Subramanian, E.E. Wolf, P.V. Kamat, J. Am. Chem. Soc. 126 (2004) 4943–4950.
[14] V. Iliev, D. Tomova, L. Bilyarska, G. Tyuliev, J. Mol. Catal. A: Chem. 263 (2007) 32–38.
[15] X.G. Hou, J. Ma, A.D. Liu, D.J. Li, M.D. Huang, X.Y. Deng, Nucl. Instrum. Methods B 268 (2010) 550–554.
[16] P. Xiao, B.B. Garcia, Q. Guo, D.W. Liu, G.Z. Cao, Electrochem. Commun. 9 (2007) 2441–2447.
[17] K.M. Youssef, C.C. Koch, P.S. Fedkiw, Electrochim. Acta 54 (2008) 677–683.
[18] G.N. Xiao, S.Q. Mao, Acta Chim. Sin. 68 (2010) 1272–1276.
[19] Z.H. Zhang, Y. Yuan, L.H. Liang, Y.X Cheng, J. Hazard. Mater. 158 (2008) 517–522.

[20] Y.Z. Lei, G.H. Zhao, M.C. Liu, Z.N. Zhang, X.L. Tong, T.C. Cao, J. Phys. Chem. C 113 (2009) 19067–19076.
[21] A.I. Mardare, A. Ludwig, A. Savan, A.D. Wieck, A.D. Hassel, Electrochim. Acta 54 (2009) 5171–5178.
[22] N. Baram, Y. Ein-Eli, J. Phys. Chem. C 114 (2010) 9781–9790.
[23] L.V. Taveira, A.A. Sagues, J.M. Macak, P. Schmuki, J. Electrochem. Soc. 155 (2008) C293–C302.
[24] P. Hartmann, D.K. Lee, B.M. Smarsly, J. Janek, ACS Nano 4 (2010) 3147–3154.
[25] S.X. Liu, Z.P. Qu, X.W. Han, C.L. Sun, X.H. Bao, Chin. J. Catal. 25 (2004) 133–137.